Pergamon

Int. J. Heat Mass Transfer. Vol. 38, No. 2, pp. 351–362, 1995

0017-9310/95 $9.50+0.00

0017-9310(94)00159-6

Convection patterns in a triangular domain

HAYDEE SALMUN†

Robert Hooke Institute, The Observatory, Clarendon Laboratory, Parks Road, Oxford OX1 3PU, U.K.

(*Received* 29 *January* 1993 *and in final form* 18 *March* 1994)

Abstract—The phenomenon of natural convection in trapezoidal enclosures where upper and lower walls are not parallel, in particular a triangular geometry, is re-examined over a parameter domain in which the aspect ratio of the enclosure ranges from 0.1 to 1.0, the Rayleigh number varies between 10^2 and 10^5, and the Prandtl numbers correspond to air and water. The time dependent, two-dimensional non-linear problem is solved numerically and the results confirmed by independent methods. It is found that the numerical experiments verify the flow features that are known from theoretical asymptotic analysis of this problem (valid for shallow spaces) *only* over a certain range of the parametric domain, and that this solution breaks down as the Rayleigh number is increased beyond 3×10^3, when a bifurcation takes place and a new steady state is achieved, that of a multi-cellular type. The transient numerical experiments show that in the present parametric domain the single-cell circulation is not stable with respect to the Bénard instability one expects in fluid layers heated from below. This result is supported by recent experimental and numerical results reported on this problem.

1. INTRODUCTION

The transport of heat and mass by buoyancy-induced circulations is a mechanism relevant to many physical systems. In particular, the problem of convective motions in confined geometries has many geophysical applications and is of increasing importance given recent concern with environmental problems. Examples of these applications are differential heating and cooling in lakes and estuaries, flow in porous media and natural convection in reservoir sidearms. For a review on natural convection in enclosures and its applications in science and technology see ref. [1]. The stability of the flow in confined rectangular enclosures has also received considerable attention in recent years [2], as have convective flows in non-rectangular geometries [3, 4] and in tilted cavities saturated with porous material [5] (in which a thorough review of the literature can be found).

The wedge-like geometry may be used to study near-shore thermal circulation or processes related to boundary mixing in shallow lakes or other shallow domains with a sloping bottom. For the problem of turbulent mixing near boundaries, the equations for the mean flow in the turbulent boundary layer, under suitable assumptions, are the same as those that describe the classical convection problem in a viscous fluid, with the molecular coefficients replaced by turbulent exchange coefficients and the closest geometrical approximation to a laboratory or field situation involving a sloping wall is a wedge region contiguous to another of rectangular shape. The work reported here originated from an attempt to use a suitable model to study these problems, the first step being that of reproducing known results. The work of ref. [6], hereafter referred to as PB, seemed to provide the desired model, but failure to reproduce their results led to a series of studies on the nature of this convective system and to a re-examination of their conclusions.

PB's work investigated the fluid dynamics inside a triangular enclosure with cold upper wall and warm horizontal bottom wall. They applied the asymptotic methods of ref. [7] to find the approximate steady-state circulation pattern and temperature structure inside a triangle, valid when the aspect ratio of the enclosure is vanishingly small. This circulation consists of a single elongated cell driven by the cold upper (sloping) wall, and the net heat transfer in this limit is dominated by pure conduction. They then examined the transient regime using a scaling analysis of the type due to ref. [8], valid for Prandtl numbers of order one or larger and for enclosed rectangular cavities with differentially heated end walls. The scaling arguments of PB led to the criteria for the existence of distinct thermal and viscous layers along both walls in the steady state, a characteristic of convective regimes, and showed that, when these boundary layers exist, the layers along the top and bottom boundaries develop simultaneously and the top layers reach a steady state after the bottom layers. Lastly, they performed numerical simulations of the transient behaviour of the system for aspect ratios equal to 0.2, 0.4 and 1.0; Grashof numbers equal to 10, 10^3 and 10^5 and Prandtl numbers of 0.72 (for air) and 6.0 (closer to that of water). PB concluded that the numerical experiments confirmed the flow features described by their theoretical analysis of the problem for this range

†Present address: Department of Geography and Environmental Engineering, The Johns Hopkins University, Baltimore, MD 21218-2686, U.S.A.

NOMENCLATURE

A	aspect ratio, H/L
Gr	Grashof number, $g\alpha(T_h - T_l)H^3/\nu^2$
g	acceleration due to gravity
H	enclosure maximum height
L	enclosure horizontal extent
M	mesh size
Nu	Nusselt number
$Nu_{t\to\infty}$	steady-state value of the Nusselt number
Pr	Prandtl number, ν/κ
Ra	Rayleigh number, $g\alpha(T_h - T_l)H^3/\nu\kappa = Gr \times Pr$
Ra_{crit}	critical Rayleigh number
t	non-dimensional time, $t'\nu/H^2$
t'	time
T	non-dimensional temperature, $(T' - T_l)/(T_h - T_l)$
T'	temperature
T_h	temperature of the warm horizontal wall
T_l	reference temperature, that of the cold sloping wall
u, v	non-dimensional velocity components: $u = u'H/\nu, v = v'H/\nu$
u', v'	velocities
x, y	non-dimensional coordinate system: $x = x'H, y = y'H$
x', y'	Cartesian coordinate system, y' vertical
$\Delta x, \Delta y$	grid spacing.

Greek symbols

α	coefficient of thermal expansion
κ	thermal conductivity
ν	kinematic viscosity
ω	non-dimensional vorticity, $\omega' H^2/\nu$
ψ	non-dimensional stream function, ψ'/ν
ψ'	stream function
ψ_{max}	maximum value of stream function
$\psi_{max/min}$	maximum/minimum value of stream function
ψ_{min}	minimum value of stream function
ω'	vorticity.

of the parameters; that the flow structure at steady state was characterized by the single-cell circulation pattern, that the convective-heat transfer mechanism was not the dominant one even at high Gr, and that the flow pattern was stable with respect to the Bénard instability expected in fluid layers heated from below.

This work seemed then to yield an interesting conclusion: while the enclosure is cooled from above and from the side (i.e. along the sloping wall) the observed natural circulation is of the type associated with enclosures heated from the side; namely, a single-cell as in a long rectangular enclosure with differentially heated vertical walls, even at the highest value of Rayleigh number they considered. The conclusion on the stability of the steady-state solutions was mainly based on direct numerical simulations and in support of some of their results they cite the agreement with the criteria derived from the scale analysis of the transient regime. However, a close examination of their scale analysis shows that some conditions do not rigurously follow from the assumptions, which may affect quantitative comparisons. For example, PB concluded that even for the highest Ra of $O(10^5)$, the dominant heat-transfer mechanism seemed to be conduction when Pr is of $O(1)$. In support of this conclusion, they refer to its agreement with the criterion for the existence of distinct boundary layers along the walls, which they had found to be that $Ra^{1/4}A^{1/2} > 1$. In their simulation with high Ra they concluded that a value of $Ra^{1/4}A^{1/2} \approx 7$ is not appreciably larger than unity, hence, supporting the lack of existence of boundary layers. Apart from the fact that an $O(10)$ number is appreciably larger than unity (especially when considering that for the lower values of Ra they used, this combination of parameters yields values of 2 and 3 which can be reasonably considered close to unity), the criterion itself is highly arguable. Following Patterson and Imberger [8], the condition for distinct thermal boundary layers requires that $Ra^{1/4}A^{-1/2} > 1$ or equivalently $Ra > A^2$, and not the one mentioned above, as PB incorrectly state. The condition for distinct viscous boundary layers yields $Ra > (PrA)^2$ and the condition that a boundary layer along the sloping wall becomes convective before heat can be transferred by conduction throughout the cavity requires that $Ra^{1/2}A > 1$. All of these conditions are amply satisfied with the values of the parameters used in PB's work, the latter condition being approximately equal to 54 with Ra of $O(10^5)$, lending support to the conclusion that the dominant heat-transfer mechanism is convection, contrary to PB's findings.

The present paper reports on the numerical results obtained from a detailed analysis of basically the same problem, which led to different conclusions. The response of the two-dimensional, non-linear system to changes in all parameters was explored numerically using two different schemes. In Section 3, the numerical model and numerical methods are described and in Section 3 the results are discussed in detail. Finally, some concluding remarks are stated in Section 4.

2. NUMERICAL EXPERIMENTS

2.1. *The numerical model*

The non-dimensional equations governing the conservation of mass (volume), vorticity and energy at

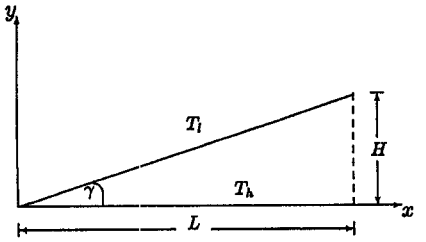

Fig. 1. A schematic diagram of the model geometry and definition of coordinate system.

every point in the two-dimensional enclosure of Fig. 1 are:

$$\frac{\partial u}{\partial x}+\frac{\partial v}{\partial y}=0, \tag{1}$$

$$\frac{\partial \omega}{\partial t}+\frac{\partial}{\partial x}(u\omega)+\frac{\partial}{\partial y}(v\omega)=Gr\frac{\partial T}{\partial x}+\left(\frac{\partial^2}{\partial x^2}+\frac{\partial^2}{\partial y^2}\right)\omega, \tag{2}$$

$$\frac{\partial T}{\partial t}+\frac{\partial}{\partial x}(uT)+\frac{\partial}{\partial y}(vT)=\frac{1}{Pr}\left(\frac{\partial^2}{\partial x^2}+\frac{\partial^2}{\partial y^2}\right)T. \tag{3}$$

The non-dimensional vorticity, velocity and stream function fields are related by:

$$u=\frac{\partial \psi}{\partial y}\quad v=-\frac{\partial \psi}{\partial x}\quad \omega=\frac{\partial v}{\partial x}-\frac{\partial u}{\partial y}=-\nabla^2\psi. \tag{4}$$

The non-dimensionalisation scheme is the same as that used by PB and is summarized in the Nomenclature.

The system of equations (1)–(4) is subject to the following conditions.

(a) Initially the fluid is at rest and the temperature is uniform everywhere. At time $t=0$ the cavity is suddenly cooled from the top by decreasing the temperature of the sloping wall.

(b) At the bottom and top rigid boundaries, $y=0$ and $y=Ax$, respectively, the flow is subject to no-slip so that $u=0=v$; $\psi=0$ there, and these boundaries are kept at a constant temperature of $T=1.0$ and $T=0.0$, respectively (perfectly conducting walls). At the centre of symmetry, $x=A^{-1}$, the flow is subject to slip; $u=0$; $\psi=0$; $\psi=0.0$ there, while $\partial T/\partial x=0.0$ (insulating wall).

2.2. *Numerical methods*

The triangular region sketched in Fig. 1 was covered with an $M\times M$ grid. The grid spacing $(\Delta x,\Delta y)$ was chosen such that $\Delta y/\Delta x=A$, hence all uppermost points lie on the sloping boundary. On this grid, two different numerical schemes were used. The first scheme was implemented in an attempt to reproduce PB's results using the same techniques that the authors reported, and the second to provide an independent solution to the problem. The primary concern of this paper is to concentrate on the solutions to the convective problem rather than on a detailed numerical comparison of the two schemes. However, the disagreement between the solutions presented here using either scheme and those obtained by PB indicated that careful and extensive tests of the numerical techniques had to be performed. This was important not only to validate the present solutions, but also to rule out the possibility that the differences in results were due to numerical details. In this subsection, the numerical schemes will be briefly summarized and their differences addressed within this context.

(a) *Numerical schemes.* Scheme 1 was implemented following the general outline reported by PB for their numerical scheme. It used a second-order central differences scheme to approximate spatial derivatives at the interior grid points except in the non-linear terms, where a second-order upwind differencing scheme was used. An explicit, one-step forward differencing scheme was then used to integrate the vorticity and temperature equations in time. The program used was based directly on the numerical scheme detailed in ref. [9, §4.6, p. 359], adapted to the present geometry. Scheme 2 used the more accurate leapfrog method for time differencing, as well as central differencing for all spatial derivatives, including the non-linear terms. On average it was found that this scheme was only slightly more costly than scheme 1. In both schemes 1 and 2, the elliptic Poisson equation (4) for the stream function ψ was solved using the successive over-relaxation method (SOR). A general formulation of the SOR method can be found in Chapter III of ref. [10], in particular a detailed discussion on the relaxation parameter, a factor that controls the convergence of the solution and whose 'optimum' value depends in general on the mesh, the shape of the domain and the type of boundary conditions. The accuracy of the SOR method for the present problem, as well as the goodness of the over-relaxation parameter which had to be found by trial and error, was checked by using standard NAGLIB subroutines. The direct method to solve the discretized form of equation (4) involves solving the system of simultaneous linear algebraic equations that results when using finite differences. The two methods yielded the same solutions well within the tolerance level of error associated with the overall numerical scheme.

Boundary conditions are only available in an explicit form for the temperature, the velocity and the stream function fields, while solutions are sought for the vorticity and energy equations. The evaluation of vorticity at walls is extremely important because at a no-slip wall vorticity is produced and it is this vorticity that, when diffused and advected away from boundaries, drives the problem. See again ref. [10] for an exhaustive general discussion on this matter. In principle and theory, from known boundary values of either velocity or stream function fields plus their computed values at all interior points, the vorticity at the boundaries can be evaluated. This indirect method

may introduce errors, and some care must be exercised so that the goodness or/and accuracy of this approximation does not influence significantly the overall accuracy of the numerical scheme. The values of vorticity on rigid boundaries ($\omega = 0$ along the axis of symmetry $x = A^{-1}$ where slip is allowed) were computed using the velocity fields, as defined in equation (4), and the known boundary conditions on the velocity field. This equation was approximated using a three-point forward/backward differencing scheme having a truncation error of $O(\Delta x^2, \Delta y^2)$. Other alternatives were tested in the present geometry and in cases where a known solution to an equivalent problem was available. It was found that the method adopted here yielded the best results.

In summary, both schemes here, as well as PB's, are second-order accurate and the difference between them basically rests on the manner of approximating the non-linear terms. The main concern with scheme 1, after testing solutions for the stream function and the boundary conditions on vorticity, is the fact that upwind differencing schemes, although stable and monotonic, introduce significant false diffusion. On the other hand, methods that eliminate false diffusion may produce unphysical overshoots and undershoots, and lead to oscillations and divergence. This is especially the case for highly convective flows, for which false diffusion may seem a desirable feature. It is also well known that false diffusion may suppress useful information on both the approach to steady state and the steady-state flow itself [11–13] (and many others referenced therein). So far there does not seem to exist a universal numerical scheme to be used for convection problems, and, in the light of the tests and comparisons detailed below, scheme 2 was preferred over scheme 1.

(b) *Comments on resolution and comparison of schemes.* Resolution tests were carried out using both schemes and three, sometimes four, different (uniform) mesh sizes. The aspect ratio of the enclosure was fixed at $A = 0.2$, the Prandtl number at $Pr = 0.72$, and grids of $(\Delta x, \Delta y) = (0.25, 0.05)$, (0.125, 0.025), (0.083, 0.0166) and (0.0625, 0.0125) were tried for different values of Gr, since the adequacy of a given resolution depends on the flow regime; which in turn (for a fixed A and Pr) will depend on Gr. Results will be summarized with single plots of one descriptive quantity, such as the maximum value of ψ and its manner of approaching steady state or the quantity that describes the heat transfer in the cavity, the Nusselt number Nu, given by:

$$Nu = -A \int_0^{A^{-1}} \left(\frac{\partial T}{\partial y}\right)_{y=0} \mathrm{d}x. \tag{5}$$

For $Gr = 10^3$, the solutions were unaffected both by the choice of scheme and by grid resolution as shown in Fig. 2(a), where the approach of ψ_{max} to steady state for all resolutions using scheme 1 is plotted. Virtually the same figure (not shown here) is

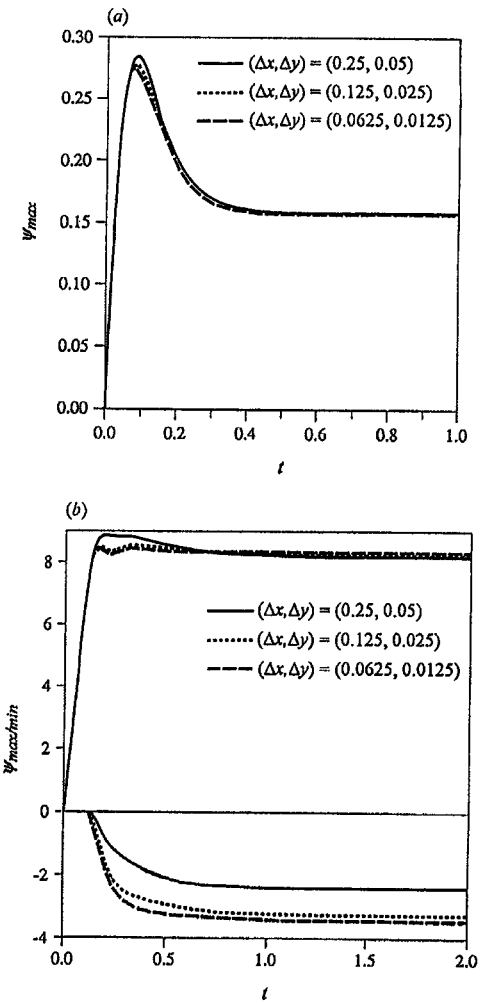

Fig. 2. Summary of resolution tests. (a) $Gr = 10^3$, $Pr = 0.72$ and $A = 0.2$. Time evolution of ψ_{max} as calculated using scheme 1 and all different resolutions tested. (b) $Gr = 10^4$, $Pr = 0.72$ and $A = 0.2$. The time evolution of $\psi_{max/min}$ as calculated using scheme 2 and the indicated resolutions.

obtained when using both schemes with a $(\Delta x, \Delta y) = (0.125, 0.025)$ mesh. For $Gr = 10^4$, the lowest resolution was inadequate, as illustrated in Fig. 2(b), where results obtained with scheme 2 are used. It is also clear in this case that the improvement in resolution beyond $(\Delta x, \Delta y) = (0.125, 0.025)$ does not improve the solution significantly, while increasing significantly the cost of a simulation. The results using scheme 1 for $Gr = 10^5$ yielded a similar plot, in a higher range of numerical values, and is not reproduced here. It is clear from the figures that the $(\Delta x, \Delta y) = (0.125, 0.025)$ mesh is adequate for the purposes of the present analysis and it was adopted subsequently.

In view of these differences, associated primarily with changes in Gr, it was instructive to follow the changes in the steady-state values of $\psi_{max/min}$ and Nu using both schemes as Gr changed gradually between 10^3 and 10^4 in order to observe when these values

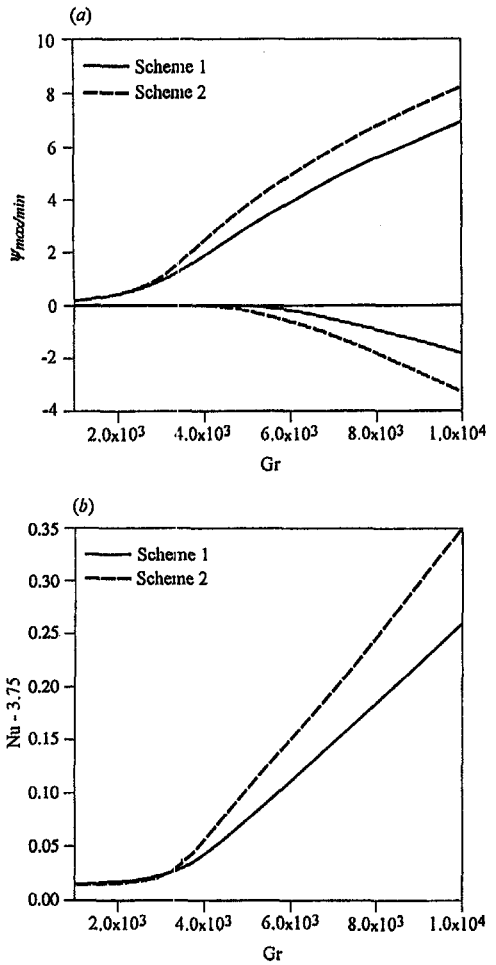

Fig. 3. Summary of comparison of the two numerical schemes, with $Pr = 0.72$ and $A = 0.2$. (a) Steady-state values of $\psi_{max/min}$ as a function of Gr, for values of Gr in the vicinity of a bifurcation. (b) Same as (a) but for steady-state values of Nu as a function of Gr. [For reasons of scale, values of $(Nu-3.75)$ were used along the ordinate.]

began to diverge. The results are shown in Fig. 3(a) and (b) for $\psi_{max/min}$ and Nu, respectively. It can be seen from this figure that solutions become significantly different as Gr is increased beyond a critical value of about 4×10^3, where the system undergoes a bifurcation, and that the difference between numerical solutions obtained with the two schemes, although large, remains approximately constant after a value of $Gr \approx 5 \times 10^3$. This type of test was also performed at a higher resolution, and similar plots were obtained (not reproduced here). Increasing the resolution with scheme 2 yielded curves that were practically indistinguishable from those shown in Fig. 4, with very small differences in the numerical values of ψ_{min} only, while curves obtained with scheme 1 did change appreciably. These changes, however, amounted to a narrowing of the difference in results obtained with the two schemes, bringing the curves obtained with higher resolutions much closer together. The change in flow

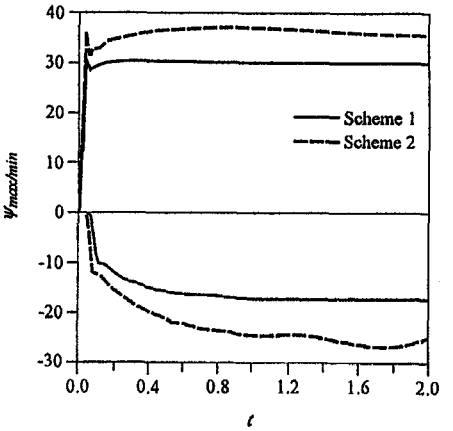

Fig. 4. Summary of comparison of the two numerical schemes, with $Pr = 0.72$, $A = 0.2$ and $Gr = 10^5$ showing the variation of $\psi_{max/min}$ with time.

structure when using scheme 1 with a higher resolution occurs at a lower value of Gr, closer to that at which changes occur with scheme 2. These tests, in turn, lend further support to the suitability of a (0.125, 0.025) mesh for this study, as well as to the validity of solutions obtained with the more accurate numerical scheme 2.

Finally, results from the two schemes were compared for values of Ra (or Gr) of $O(10^4, 10^5)$ and these are summarised in Fig. 4 where curves of the time evolution of ψ_{max} and ψ_{min} for the case $Gr = 10^5$ only, are shown. Although numerical differences are large, especially in the values of ψ_{min}, both schemes yield results that agree very well at earlier times, before the single cell breaks down, consistent with the agreement throughout when $Gr = 10^3$, and with $Gr = 10^4$ these differences do not imply significant differences in the flow structure, while with $Gr = 10^5$ they do. With $Gr = 10^5$ the long-term behaviour of $\psi_{max/min}$ (especially that of ψ_{min}) is indicative of undulations about the asymptotic steady-state field while both curves were 'flat' for large values of t when $Gr = 10^4$. For both values of Gr, scheme 2 gives more accurate details of the structure of the flow everywhere, especially in the regions close to the tip of the enclosure, where more cells could plausibly develop with time, at a slower rate, at high values of Gr. The steady state obtained with both schemes using $Gr = 10^4$ is that of three well-developed convective cells, while with $Gr = 10^5$ numerical differences are larger and scheme 1 yields a steady state with five convective cells while scheme 2 yields one with seven cells. These results will be discussed in more detail in the next section. Long time integrations were performed with both schemes, especially scheme 2, to ensure that the time steps and mesh size used did not present problems with numerical instabilities with these values of Gr. The results of these tests give a consistent general set of solutions in the range of parameters considered in this work.

In summary, using both schemes it was found that the flow can bifurcate into a multi-cellular regime as Gr is increased, in which case lower resolutions are insufficient. Both schemes produce qualitatively (and quantitatively as well, when the resolution is increased) the same bifurcation, a transition in the flow structure that occurs at a critical values of Gr between 4 and 5×10^3. Although with air a (0.125, 0.025) grid was deemed adequate and used subsequently, the persistance of the same solution at higher resolution using both schemes was confirmed by numerical simulations. In no case were PB's results reproduced.

3. NUMERICAL RESULTS

This section discusses the numerical experiments that were carried out to test and analyse the response of the system to changes in Ra, A and Pr. In the numerical work the Grashof number $Gr = Ra/Pr$ was used and results will be discussed in terms of either non-dimensional parameter, particularly in the case of air since $Pr \approx 1$. All results discussed below were obtained using scheme 2 described in Section 2, unless otherwise specified.

3.1. *The Rayleigh number*

The following numerical experiments were directed at studying the changes in the system to changes in Ra, with a fixed value of $Pr = 0.72$, and at analysing the stability of the asymptotic solution obtained by PB. The steady-state asymptotic solution, valid in the limit $A \to 0$ for an enclosure with a flat top boundary, represents to first order slightly tilted isotherms which give rise to a steady counterclockwise circulation. This circulation is such that the entire fluid is slowly entrained in the slow gyre that fills the entire domain. The isotherm pattern indicates that, in this limit, conduction is the dominant mechanism for the heat transfer across the cavity. PB did not analyse the stability of this solution but their numerical results seemed to indicate that this basic solution was characteristic of all their simulations, at least qualitatively, up to a Ra of $O(10^5)$. With $Gr = 10^3$ the aspect ratio A was varied between 0.01 and 0.2 to verify the validity of the asymptotic theory. They found that, except for small differences in the numerical values of the steady-state fields, changes in A did not affect the basic steady solution which corresponded to that predicted by the asymptotic theory in this range of the parameters. This was also confirmed by the present study. As Ra was increased, however, this solution was no longer attainable, as discussed in details below.

(*a*) *Experiment* 1: Gr = 10^3, A = 0.2. Two runs were compared: one with the fluid initially at rest and the other with the initial flow given by the asymptotic solution. The runs yielded basically the same final steady state, results being slightly different at earlier times in the integration as expected. The steady state was reached in both cases, starting from rest or from the asymptotic field, at a non-dimensional time $t \approx 0.5$. Incidentally, this was also the case when the scheme 1 described in Section 2 was used. A close inspection of the solutions at $t \approx 0.2$, the dimensionless time reported by PB as when steady state was reached, indicated that the fields were still changing considerably, although this was not as significant a change as occurs with higher values of Ra at this same time. To test for changes due to different boundary conditions, a simulation was performed with the no-slip condition on the vertical plane at $x = A^{-1}$. This had no effect on the general characteristics of the numerical solution with these values of the parameters, producing only minor changes in the numerical values of the steady-state fields. The temperature and flow fields at steady state for this case are shown at the top of Fig. 5 [cf. Fig. 5(a)]. The approach to steady state was monotonic, the isotherms being slowly spread apart to their final tilted, evenly separated position.

(*b*) *Experiment* 2. As the value of Gr was increased from 10^3 the single-cell solution became unstable and a new steady state was achieved with three counter-rotating convective cells occupying the entire cavity. The onset of multi-cellular motion was studied numerically and Fig. 5 shows a summary of these simulations for particular values of Gr, although results were analysed for very small increments in Gr. Table 1 summarizes the salient features in this figure, showing the values of $\psi_{\min}$ (the counter-circulating cell) and $\psi_{\max}$ (the main cell) as the Gr is increased and after the steady state has been reached. It can be seen that with $Gr = 3 \times 10^3$ the cell that occupied the entire cavity moves slightly towards the left side as it intensifies, creating a relatively large stagnant zone at the opposite end where the isotherms are still nearly parallel. As Gr is increased to 4×10^3 this process continues further with the flow in the main cell becoming more intense and the isotherms at the higher end of the cavity beginning to show clearly the effects of convective motions while the single cell remains. The multi-cell circulation starts to develop as Gr is increased past that value and the counter-circulating cell, although weak, is clearly detectable at $Gr = 4.5 \times 10^3$. With $Gr = 5 \times 10^3$ this cell is well developed, with a flow intensity of the same order of magnitude as that of the single cell with $Gr = 10^3$. In fact, bifurcation occurs at a value of Gr between 4.009×10^3 and 4.01×10^3, which corresponds to a value of $Ra_{\text{crit}} \approx 2886.84$. This result was already apparent in the plots of Fig. 3, where the sudden changes in the values of $\psi_{\max/\min}$ and Nu with small changes in Gr about 4×10^3 indicated the sudden changes in the flow regime associated with a bifurcation.

(*c*) *Experiment* 3: Gr = 10^4, A = 0.2. In this case the system, which was started from a state of rest, evolves in the same manner it evolved with $Gr = 10^3$. At earlier times, a single cell occupies the entire enclosure, the flow intensifies and at a non-dimensional time $t \approx 0.125$ the primary cell occupies less than half of

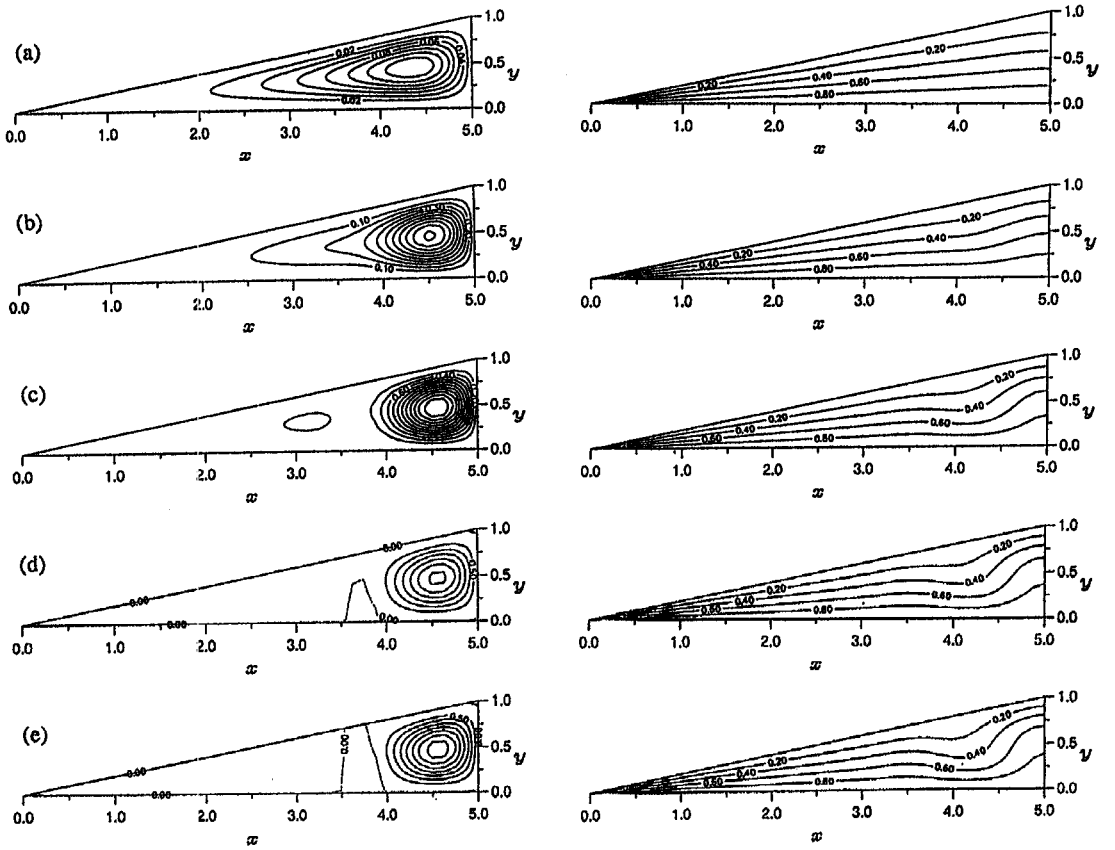

Fig. 5. Steady-state stream function (ψ, left) and temperature (T, right) fields with $Pr = 0.72$, $A = 0.2$ and (a) $Gr = 1.0 \times 10^3$, (b) $Gr = 3.0 \times 10^3$, (c) $Gr = 4.0 \times 10^3$, (d) $Gr = 4.5 \times 10^3$ and (e) $Gr = 5.0 \times 10^3$, showing the change in flow regimes, from a single cell to a multi-cellular flow, as Gr is increased. All numerical values are non-dimensional and listed in Table 1.

Table 1. Non-dimensional steady-state values of ψ_{min} and ψ_{max} corresponding to the values of Gr used in the diagrams of Fig. 5

Gr	ψ_{min}	ψ_{max}	Contour interval
1.0×10^3	0.00	0.16	0.02
3.0×10^3	0.00	1.03	0.1
4.0×10^3	0.00	2.40	0.2
4.5×10^3	−0.06	3.11	0.5
5.0×10^3	−0.21	3.76	0.5

the domain and a weak cell with flow circulating in the opposite direction begins to develop. At $t \approx 0.3$ the three-cell pattern is well established, reaching a steady state at $t \approx 0.5$. The three-cell pattern is characteristic for simulations with $Ra \approx O(10^4)$ and $A = 0.2$. As can be seen in the diagram of Fig. 6(a), the active convective cells occupy most of the region on the higher end of the cavity, (i.e. $x > 2.5$ in the figure) leaving still a considerably large zone to the left where conduction is dominant (cf. isotherms diagram). In this case as before, a change in the boundary condition along the vertical plane from no-slip to slip only produced negligible changes in numerical values of the solutions. At this value of Gr the approach to steady state is practically monotonic, although the data plotted in Fig. 2(b) seemed to indicate the presence of weak oscillations in the system before it reaches steady state and these were absent with lower Gr.

(*d*) *Experiment* 4: Gr = 10^5, A = 0.2. Three runs were compared to determine the sensitivity of the final solution to initial conditions: one with the initial fluid at rest, another with an initial flow field described by the asymptotic theory and a third one using the steady-state flow field corresponding to the single cell obtained with $Gr = 10^3$, multiplied throughout by a suitable factor to make it closer in numerical values to that solution obtained by PB. In all cases the solution reported by PB in this range of parameters could not be obtained and the single cell broke down into convective cells very early in the integration, at a non-dimensional time $t \approx 0.05$ or less. There were some differences in the numerical values of these solutions but these were deemed insignificant.

Figure 6(b) shows that the steady-state fields for $Gr = 10^5$ are those of a convection-dominated flow. The approach to steady state was oscillatory. At this value of Gr there are seven fully developed convective cells in the steady state. The initial large counter-

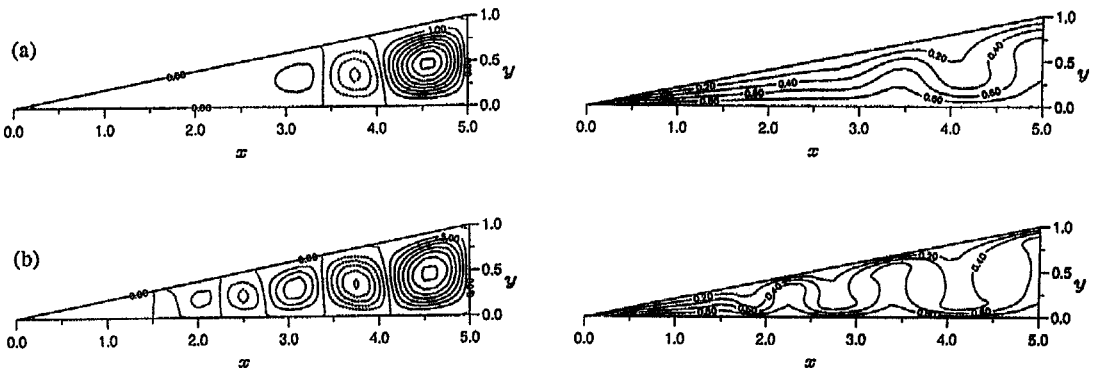

Fig. 6. Steady-state fields, stream function (ψ, left) and temperature (T, right) with $Pr = 0.72$, $A = 0.2$, and (a) $Gr = 10^4$ and (b) $Gr = 10^5$, showing the differences between the two convecting regimes. All numerical values are non-dimensional. The values of ψ range between -3.27 and 8.22 with contour intervals of 1 in (a), and between -25.16 and 35.70 with contour intervals of 5 in (b).

clockwise cell has been slowly pushed towards the rightmost end side and the appearance of smaller cells towards the left end of the cavity has eliminated almost entirely the large stagnant zone present in the case of Fig. 6(a). The boundary condition on the boundary $x = A^{-1}$ was changed to requiring no-slip and, as in the previous cases, it was found that the basic flow structure remained unaffected. A weakly counter-circulating small cell formed at the top corner of the right side of the cavity and numerical values of all fields were different but of the same order. These numerical differences were slightly larger with the increased value of Gr. The number of cells, the approach to steady state, the flow intensity and the heat transfer rate all remained very close to the case with slip along that boundary, because the small new cell did not distort the large cell and it did not touch the hot bottom wall. In ref. [4], where solutions to a similar problem that are in qualitative agreement with the present ones are discussed, it is suggested that this difference in boundary conditions is the possible explanation of their discrepancies with PB's results. However, the present results indicate rather strongly that the discrepancies are not likely to be related to these differences in boundary conditions.

3.2. *The aspect ratio*

As mentioned earlier, with a value of $Ra \approx 10^3$ the changes in the aspect ratio A that were tested in this study did not affect the circulation in the enclosure. Simulations carried out with a higher value of Ra and different values of A showed, however, that changes in A do affect the flow pattern and temperature fields significantly. In this analysis a fixed Ra of 0.72×10^5 was used and numerical experiments were conducted with values of $A = 0.1$, 0.15, 0.3, 0.5 and 1.0, adding to the data obtained with $A = 0.2$.

For all values of A except $A = 1$, the system evolved in time as with $A = 0.2$ described above. The flow structure changed with changes in A as depicted in the diagrams of Fig. 7, where the steady-state fields obtained for the different values of A indicated in the figure caption are shown. The main features in this figure are summarized in Table 2. The number of cells that developed depended strongly on A, increasing with decreasing A, the cells becoming more comparable in size the smaller A became. Since cells developed farther into the lower side of the cavity as A decreased, the stagnant region near the tip became much smaller. Although results are shown in the figure at $t \approx 1.0$, integrations were carried out for long enough times, particularly those with the smaller values of A, to verify that the flow structure would remain as that depicted in the figure. Time and space resolution were also tested for the small aspect ratio experiments. It is worth noting that although the three-cell circulation characterizes the steady states with $A = 0.5$ and $Ra = 0.72 \times 10^5$ and that, with $A = 0.2$ and $Ra = 0.72 \times 10^4$, their size and the intensity of the flow associated with them are significantly different. These differences imply significant differences in the associated heat transfer, as can be seen from comparing their respective isotherm diagrams as well as their respective Nu vs time curves.

The case $A = 1$ is one of a single-cell, steady-state circulation, as in the experiments reported by PB, although the agreement in numerical values is rather poor. In the present experiments, the maximum value reached by the stream function at steady state is more than three times larger than that obtained by PB and the temperature fields were not reported there. It should be noted that this experiment was also carried out with scheme 1 and that the results obtained with that numerical scheme were basically the same, consistent with the agreements between results from both schemes, as detailed in Section 2. The steady-state isotherm pattern for $A = 1$ in Fig. 7 indicates that this solution cannot be stable. In particular, it is not stable to small departures from $A = 1$, and as A is decreased the single cell was no longer attainable. Although a

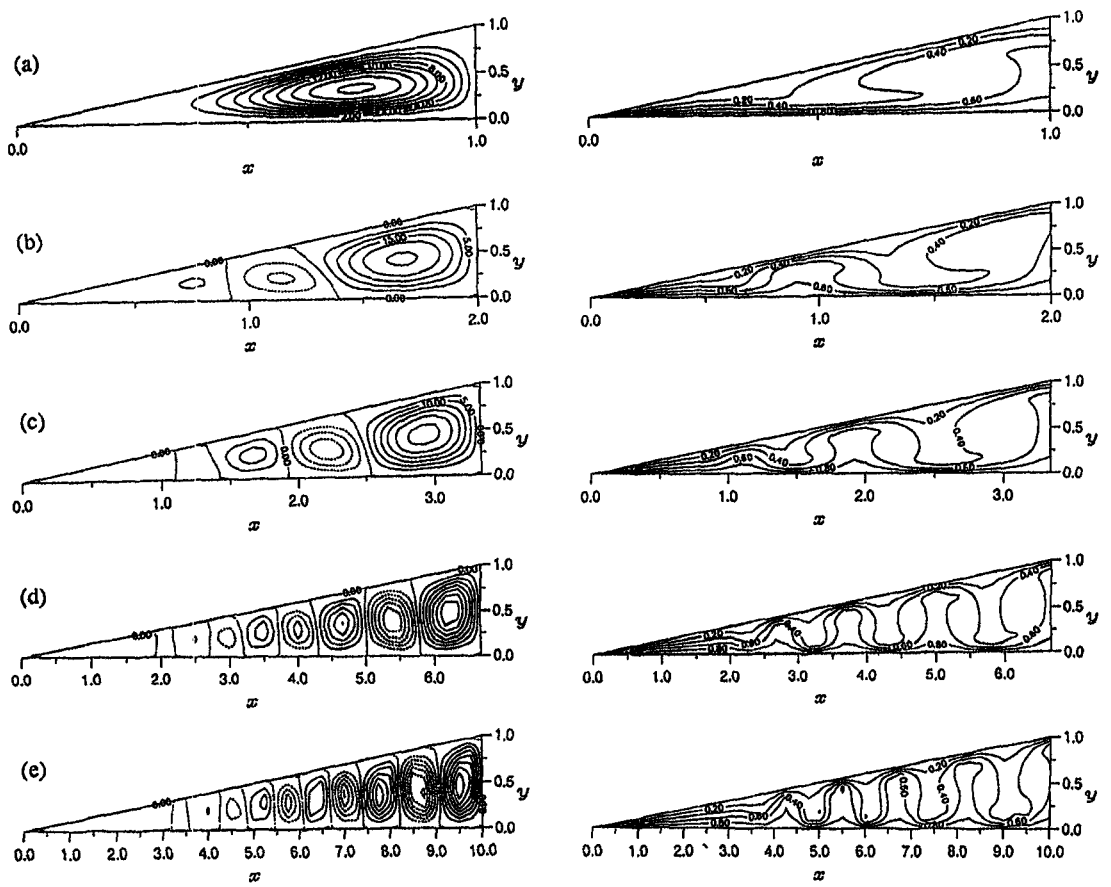

Fig. 7. Steady-state stream function (ψ, left) and temperature (T, right) fields with $Pr = 0.72$, $Gr = 10^5$ and (a) $A = 1.0$, (b) $A = 0.5$, (c) $A = 0.3$, (d) $A = 0.15$ and (e) $A = 0.1$, showing the change in flow structure as the aspect ratio is decreased. All numerical values are non-dimensional and listed in Table 2.

Table 2. Non-dimensional steady-state values of ψ_{min} and ψ_{max} corresponding to the values of A used in the diagrams of Fig. 7

A	ψ_{min}	ψ_{max}	Contour interval
1.00	0.00	18.41	2.0
0.50	−11.02	25.85	5.0
0.30	−18.30	32.21	5.0
0.15	−29.90	39.39	5.0
0.10	−30.55	39.89	5.0

numerical stability analysis when varying A was not performed in the same detailed manner as that performed with changes in Ra, the results presented here indicate that a rich pattern of bifurcations takes place in this physical system as the different parameters that control its behaviour vary. The study of such bifurcation patterns is beyond the scope of this paper and it will be pursued elsewhere.

Direct quantitative comparisons with the results reported by ref. [4] are not possible because of the differences in geometry, range of parameters and different boundary conditions they used in their numerical experiments. It is useful to note, however, the qualitative similarities in some results. The present case with $Ra = 0.72 \times 10^5$ and $A = 0.5$ is qualitatively equivalent to their numerical simulations at $Ra = 10^4$, with $A = 4$ (defined using their nomenclature) and with the cold plate inclined by about 25° with respect to the horizontal. The three-cell circulation they obtained for this simulation persisted up to a value of $Ra = 8 \times 10^5$, in the present notation. For the largest angles they used, the relationship between the angle of inclination and the aspect ratio is approximately the same as the one defined in here, and it is interesting to note that with an angle of 20°, which is the closest analogue to an aspect ratio of about 0.4 in here, they find a steady state with five convective cells. Their work also seems to indicate that a decrease in aspect ratio for a fixed (high) Ra yields an increase in the number of cells present in the steady state.

3.3. *The Prandtl number*

The case of a cavity filled with water was also considered in several experiments. With a fixed $A = 0.2$ and $Pr = 7.1$, the values of $Gr = 10^2$, 10^3, 10^4 and 10^5 were used in the numerical simulations of this subsection and results are summarized in Figs. 8 and

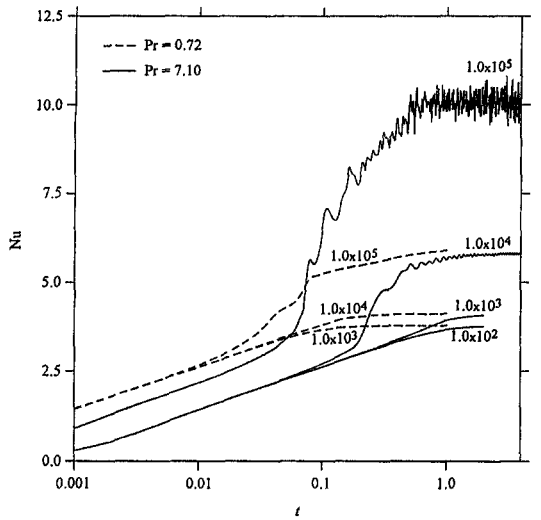

Fig. 8. The *Nu* approach to steady state for numerical experiments with $A = 0.2$, $Pr = 0.72$ and $Pr = 7.1$ and the values of Gr indicated on each curve.

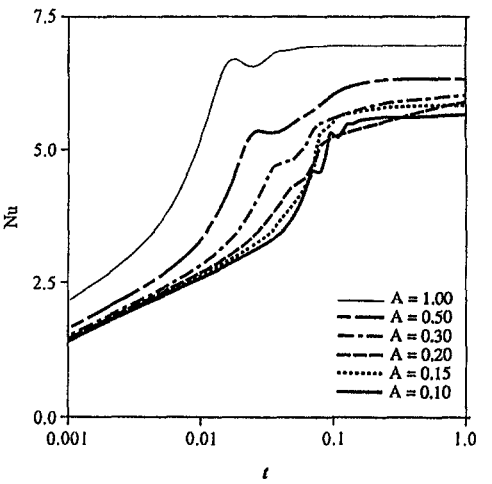

Fig. 9. The dependence of *Nu* on time for numerical experiments with $Pr = 0.72$ (air), $Gr = 10^5$ and the different values of the aspect ratio A used in this study.

10, which show *Nu* vs t and $Nu_{t\to\infty}$ vs Gr, respectively, for all these simulations. As expected, the time needed to reach steady state is greater than in the equivalent cases using air, as can be seen from comparing curves for air and water in Fig. 8.

Steady-state stream function and temperature fields were plotted in the same fashion as those shown in Figs. 5–7. For the sake of brevity, however, and in view of the close similarities in flow patterns with results using air, especially for the lower values of Gr, these plots will not be reproduced here. The flow structure with $Gr = 10^2$ and $Gr = 10^3$ is virtually identical with that of $Gr = 10^3$ and $Gr = 10^4$, respectively, with air. The difference is, as expected, in the flow velocities, which are an order of magnitude less than with air. These similarities are clear in the curves of *Nu* vs t for $Pr = 0.72$ and $Pr = 7.1$ in Fig. 8 for these values of Gr. The steady-state flow structure when $Gr = 10^4$ presents some similarities with that of $Gr = 10^5$ and $Pr = 0.72$, such as the same number of cells attained at the final state. The cell structure, however, was notably different and, as can be seen in Fig. 8, there was some evidence of low-frequency oscillations in the steady state in the case of water which were not present with air and all the values of Gr used in this study.

When Gr is increased to 10^5 with $Pr = 7.1$, numerically stable simulations were no longer possible with the grid size used so far, that of $(\Delta x, \Delta y) = (0.125, 0.025)$ also used by PB in the only case they addressed with water, and it was necessary to use a $(\Delta x, \Delta y) = (0.0625, 0.0125)$ mesh and to adjust the time stepping accordingly. In this case, unlike with air, examination of Fig. 8 shows a high-frequency oscillation about an average value of $Nu = 10$, with amplitude about 10% of the average. Examination of the stream function data showed that the cell structure was unstable, in fact resembling weak turbulence. These results indicate that further bifurcations have taken place and, although the classification of these bifurcations is not possible with the present limited numerical data, it is clear that the steady-state multicell structure is unstable in this parameter range. It should be noted that although the case of water was not as extensively tested with scheme 1 as the case of air (see Section 2), an early attempt to use that numerical scheme with water, the higher value of Gr and the (0.125, 0.025) grid also resulted in numerical instabilities that developed at a later time in the integration.

3.4. *Summary of heat transfer calculations*

The dependence of the Nusselt number on time for all the experiments with $A = 0.2$ and all different values of Gr with $Pr = 0.72$, and $Pr = 7.1$ is shown in Fig. 8. In all cases, *Nu* rises abruptly to close to its final value, and slowly increases thereafter to its steady-state value. For high values of Gr there is some oscillation in the values of *Nu* as they approach steady state, but the behaviour reported by PB, a rise in *Nu* followed by a subsequent decrease to a final steady state value, was not observed. The circulation in the cavity with $Gr = 10^3$, although very weak, already has an effect on the overall heat transfer, as expressed in the significant departure from unity shown by the final value of *Nu*, indicating the contribution of convective motions to the overall transport of heat.

Figure 9 shows the evolution of the Nusselt number in the approach to steady state for all the different values of A. In all cases the evolution to steady state is oscillatory, the oscillations being more intense with the smaller values of A. In Fig. 9 all curves are similar except for the curves corresponding to $A < 0.2$. The steady-state values of *Nu* are not significantly different in this range of A: however, the evolution to the final state is different with $A = 0.1$ and 0.15, suggesting a possible change in the time evolution of the system

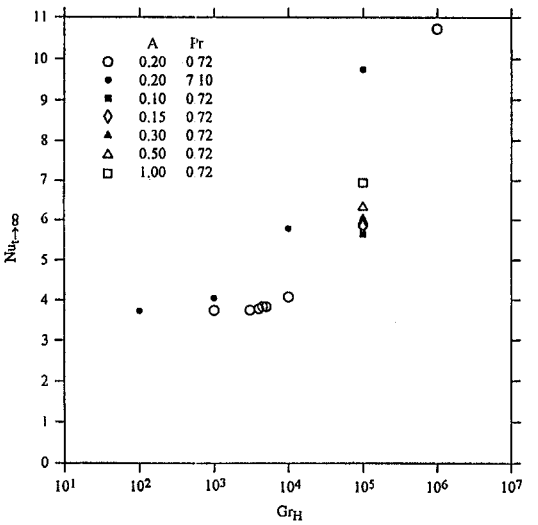

Fig. 10. Summary of numerical heat transfer results for all the experiments in this work. The steady-state value of the Nusselt number, $Nu_{t\to\infty}$, is plotted against the Grashof number for the aspect ratios and Pr values shown in the legend.

which was not investigated. As in the results of Fig. 8, Nu rises rapidly and remains thereafter close to its final value.

The effect of Gr on the final heat-transfer rate for all values of A and Pr studied in this work is summarized in Fig. 10. It can be seen from the figure that, up to a value of Gr of about 10^3, the final overall rate of transfer of heat, as measured by the steady-state value of Nu and denoted by $Nu_{t\to\infty}$, is not a function of Gr and only a weak function of Pr. In this sense, the system may be thought of as a quasi-conductive system within this parameter range (recall that for $Gr \leqslant 10^3$ changes in A did not affect the final state of the system). Beyond this point, a structure of bifurcations is taking place which depends on all three parameters, Gr, A and Pr. It should be noted that the point corresponding to $Gr = 10^5$ for water in this figure is somewhat arbitrary and has large error bars associated with it since at $t \approx 1$, when these values are computed, the system is oscillating (see Fig. 8), and this fact has not been included in the values shown. Also in the figure, results obtained with $Gr = 10^6$ in air are shown for comparison. The latter case, of which only a preliminary result from a test at that high value of Gr is shown, required a significant improvement in resolution for numerical stability. The values of $Nu_{t\to\infty}$ for the larger values of Gr are shown for a rough comparison with data at lower values of Gr.

4. CONCLUDING REMARKS

The problem of natural convection inside irregular enclosures was re-examined using a two-dimensional triangular geometry filled with air or water, with various aspect ratios and for Rayleigh numbers ranging between 10^2 and 10^5. Numerical solutions of the time dependent problem were obtained using two different numerical techniques, which while yielding different numerical values for the flow fields especially at high Ra, did not alter the general structure of the flow. The general flow structure corresponded to a single convective cell for low values of the Ra number and to a multi-cellular regime for the high values of this parameter.

Poulikakos and Bejan [6], referred to as PB and who first reported solutions to the same problem, did not define their numerical scheme precisely. They stated clearly, however, that they used the central difference formula for spatial derivatives except for the non-linear terms and that to solve the vorticity and temperature equations they used a function subprogram as that given in ref. [9]. This is the general outline that has been followed in developing the second-order scheme 1 in this paper. If, furthermore, boundary conditions were handled by PB in the manner indicated by both references they give, refs. [9, 10] in this paper, then we must conclude that scheme 1 here is as close to PB's scheme as it can possibly be, without having a numerical code for more concrete comparisons. Both schemes should have, then, the same overall order of accuracy. Different boundary conditions and their effects on the solution were tested, different ways of approximating boundary conditions on vorticity were checked, time and space resolution was amply tested so as not to rely on PB's grid size only, and, in a limited context, the sensitivity to initial conditions was also tested. All of these tests support the view that the disagreement between the solutions presented in this paper and those of PB cannot be explained in terms of differences in numerical schemes. The alternative second-order scheme 2 developed in this work, although more accurate for higher values of the Ra number, yielded the same solutions as those obtained with scheme 1. Finally, the solutions obtained in this paper for the problem of convection in a triangular enclosure is in qualitative agreement with other numerical and experimental works on similar problems in enclosures of small aspect ratio and in the same range of values of Ra.

Acknowledgements—I am indebted to Bram Hauer and Jeff Blundell for their patient help with programming and computation, and to Bram for providing the diagrams in this paper. I benefited from discussions with Joseph Tribbia, Ian Sobey, Mike Davey and Juan Rivero and their helpful suggestions. Finally, I wish to thank Robb McDonald for discussions and comments on the manuscript.

REFERENCES

1. S. Ostrach, Natural convection in enclosures, *ASME J. Heat Transfer* **110,** 1175–1189 (1988).
2. K. T. Yang, Transitions and bifurcations in laminar buoyant flows in confined enclosures, *ASME J. Heat Transfer* **110,** 1191–1204 (1988).
3. T. S. Lee, Computational and experimental studies of convective fluid motion and heat transfer in inclined

non-rectangular enclosures, *Int. J. Heat Fluid Flow* **5,** 29–36 (1984).
4. S. W. Lam, R. Gani and J. G. Symons, Experimental and numerical studies of natural convection in trapezoidal cavities, *ASME J. Heat Transfer* **111,** 372–377 (1989).
5. D. S. Riley and K. H. Winters, The onset of convection in a porous medium : a preliminary study, Harwell Report AERE R 12586 (1987).
6. D. Poulikakos and A. Bejan, The fluid mechanics of an attic space, *J. Fluid Mech.* **131,** 251–269 (1983).
7. D. E. Cormack, L. G. Leal and J. Imberger, Natural convection in a shallow cavity with differentially heated end walls. Part 1. Asymptotic theory, *J. Fluid Mech.* **65,** 209–230 (1974).
8. J. Patterson and J. Imberger, Unsteady natural convection in a rectangular cavity, *J. Fluid Mech.* **100,** 65–86 (1980).
9. C. Y. Chow, *An Introduction to Computational Fluid Mechanics.* Wiley, New York (1979).
10. P. J. Roache, *Computational Fluid Dynamics.* Hermosa (1976).
11. S. V. Patankar, *Numerical Heat Transfer and Fluid Flow.* Hemisphere (1980).
12. S. V. Patankar, Recent developments in computational heat transfer, *ASME J. Heat Transfer* **110,** 1037–1045 (1988).
13. G. de Vahl Davis, Finite difference methods for natural and mixed convection in enclosures, *Proc. Eighth International Heat Transfer Conference,* San Francisco, **1.** Hemisphere (1986).